Inorganic Chemistry

ARTICLE

pubs.acs.org/IC

Polyoxomolybdodiphosphonates: Examples Incorporating Ethylidenepyridines

Abhishek Banerjee, Farah S. Raad, Nina Vankova,* Bassem S. Bassil, Thomas Heine, and Ulrich Kortz*

School of Engineering and Science, Jacobs University, P.O. Box 750561, 28725 Bremen, Germany

Supporting Information

ABSTRACT: We have synthesized and structurally characterized three pyridylethylidene-functionalized diphosphonate-containing polyoxomolybdates, $[\{Mo^{VI}O_3\}_2\{Mo^{V}_2O_4\}\{HO_3PC(O)(CH_2\text{-}3\text{-}C_5NH_4)PO_3\}_2]^{6-}$ (**1**), $[\{Mo^{VI}_2O_6\}_2\{Mo^{V}_2O_4\}\{O_3PC(O)(CH_2\text{-}3\text{-}C_5NH_4)PO_3\}_2]^{8-}$ (**2**), and $[\{Mo^{V}_2O_4(H_2O)\}_4\{O_3PC(O)(CH_2\text{-}3\text{-}C_5NH_4)PO_3\}_4]^{12-}$ (**3**). Polyanions **1**−**3** were prepared in a one-pot reaction of the dinuclear, dicationic $\{Mo^{V}_2O_4(H_2O)_6\}^{2+}$ with 1-hydroxo-2-(3-pyridyl)ethylidenediphosphonate (Risedronic acid) in aqueous solution. Polyanions **1** and **2** are mixed-valent $Mo^{VI/V}$ species with open tetranuclear and hexanuclear structures, respectively, containing two diphosphonate groups. Polyanion **3** is a cyclic octanuclear structure based on four $\{Mo^{V}_2O_4(H_2O)\}$ units and four diphosphonates. Polyanions **1** and **2** crystallized as guanidinium salts $[C(NH_2)_3]_5H[\{Mo^{VI}O_3\}_2\{Mo^{V}_2O_4\}\{HO_3PC(O)(CH_2\text{-}3\text{-}C_5NH_4)PO_3\}_2]\cdot 13H_2O$ (**1a**) and $[C(NH_2)_3]_6H_2[\{Mo^{VI}_2O_6\}_2\{Mo^{V}_2O_4\}\{O_3PC(O)(CH_2\text{-}3\text{-}C_5NH_4)PO_3\}_2]\cdot 10H_2O$ (**2a**), whereas polyanion **3** crystallized as a mixed sodium−guanidinium salt, $Na_8[C(NH_2)_3]_4[\{Mo^{V}_2O_4(H_2O)\}_4\{O_3PC(O)(CH_2\text{-}3\text{-}C_5NH_4)PO_3\}_4]\cdot 8H_2O$ (**3a**). The compounds were characterized in the solid state by single-crystal X-ray diffraction, IR spectroscopy, and thermogravimetric and elemental analyses. The formation of polyanions **1** and **3** is very sensitive to the pH value of the reaction solution, with exclusive formation of **1** above pH 7.4 and **3** below pH 6.6. Detailed solution studies by multinuclear NMR spectrometry were performed to study the equilibrium between these two compounds. Polyanion **2** was insoluble in all common solvents. Detailed computational studies on the solution phases of **1** and **3** indicated the stability of these polyanions in solution, in complete agreement with the experimental findings.

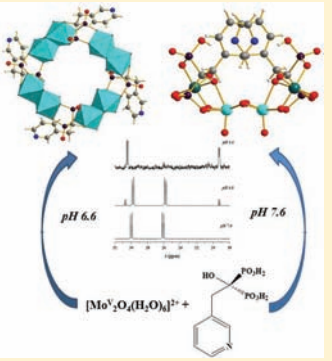

INTRODUCTION

Diphosphonic acids have been used for various potential medical applications during the last decades, especially toward the treatment of degenerative bone diseases with the first diphosphonates having been developed in the 1960s.[1] Intrinsically, diphosphonates share a similar backbone with the pyrophosphate ion ($P_2O_7^{4-}$), but the central O atom is substituted by a C atom, leading to a P−C−P backbone. This modification renders the compound more robust toward hydrolysis and allows tuning of steric and electronic properties by variation of the functional groups on the central C atom. This approach has yielded a wide variety of functionalized diphosphonates over a period of many years with improved medicinal properties. The initial generations of diphosphonates contained mainly aliphatic functional groups on the central C atom, such as Etidronate, Chlorodronate, and Alendronate.[1d] In recent years, the attention has been mostly on aromatic functionalized diphosphonates, with the aromatic ring containing one or more N atoms, such as Risedronate and Zoledronate.[1e,f]

In a similar sense, some discrete polyoxometalates (POMs)[2] have also shown interesting antibacterial and antiviral properties, indicating their potential as biologically active inorganic compounds.[3] Thus, the incorporation of diphosphonates into POMs offers possible synergistic effects, in particular with respect to medicinal applications. An important step toward the incorporation of such diphosphonates into POMs was accomplished by Pope's group with the synthesis and structural characterization of the dodecameric, saddle-shaped $[(O_3PCH_2PO_3)_4W_{12}O_{36}]^{16-}$ (as well as its pyrophosphate analogue $[(O_3POPO_3)_4W_{12}O_{36}]^{16-}$).[4a] Both compounds showed significant potency toward inhibition of the reverse transcriptase enzyme of the human immunodeficiency virus type 1 (HIV-1).[4b] Some diphosphonate-containing polyoxomolybdates,[4d] as well as the first substituted diphosphonate-containing polyoxotungstate, were also structurally characterized.[4e] In principal, the diphosphonate moiety has advantages over pyrophosphate,[4c,f] mostly because of the tendency of pyrophosphate to hydrolyze in an acidic medium. The group of Mialane and Dolbecq was able to incorporate the dinuclear $\{Mo^{V}_2O_4\}$ moiety into diphosphonate-containing POMs.[5] Several structures were obtained based on methylenediphosphonate and various templating groups such as acetate, formate, sulfite, and carbonate. The same group also prepared derivatives based on 1-hydroxoethylidenediphosphonate (Etidronic acid).[5c]

Very recently, we used diphosphonate units as scaffolds for the easy and efficient incorporation of fluorine into POMs. A simple, one-pot reaction of $\{Mo^{V}_2O_4\}$ with 1-hydroxy-2,2,2-trifluoroethylidenediphosphonate (F3-Etidronic acid) resulted in $[\{Mo^{V}_2O_4(H_2O)\}_4\{O_3PC(CF_3)(O)PO_3\}_4]^{12-}$.[6] The presence

Received: July 31, 2011
Published: October 17, 2011

dx.doi.org/10.1021/ic201652h | Inorg. Chem. 2011, 50, 11667–11675

of fluorine in the polyanion had a marked influence on its structure and led to improved solution stability. Since then, several other structures based on Etidronic acid and 4-amino-1-hydroxybutyldiphosphonate (Alendronic acid) have been reported by the groups of Wang and of Mialane and Dolbecq,[7] with a mixed-metal (Mo^{V} and V^{IV}) composition[7a] and interesting properties in optical isomerism,[7c,f] as well as medicinal activity.[7d]

We decided to further explore this area by trying to incorporate aromatic functionalities into diphosphonate–POM systems. Here we report on the reactivity of the pyridine-based 1-hydroxyethylidenediphosphonate (Risedronate) with molybdates.

RESULTS AND DISCUSSION

Synthesis and Structure. Polyanions $[\{Mo^{VI}O_3\}_2\{Mo^{V}_2O_4\}\{HO_3PC(O)(CH_2\text{-}3\text{-}C_5NH_4)PO_3\}_2]^{6-}$ (**1**), $[\{Mo^{VI}_2O_6\}_2\{Mo^{V}_2O_4\}\{O_3PC(O)(CH_2\text{-}3\text{-}C_5NH_4)PO_3\}_2]^{8-}$ (**2**), and $[\{Mo^{V}_2O_4(H_2O)\}_4\{O_3PC(O)(CH_2\text{-}3\text{-}C_5NH_4)PO_3\}_4]^{12-}$ (**3**) were synthesized in aqueous solution by the reaction of Risedronic acid with the dinuclear, dicationic $\{Mo^{V}_2O_4(H_2O)_6\}^{2+}$ unit at various stoichiometric ratios and pH values. A common structural feature of **1**–**3** is the presence of a C–O–Mo bond, resulting from deprotonation of the OH group of Risedronate and subsequent bonding to a Mo center. Polyanion **1** was synthesized by an equimolar reaction of $\{Mo^{V}_2O_4(H_2O)_6\}^{2+}$ with Risedronic acid in aqueous medium at pH 7.7, using a concentrated aqueous ammonia solution to adjust the pH, and crystallized as a guanidinium salt, $[C(NH_2)_3]_5H[\{Mo^{VI}O_3\}_2\{Mo^{V}_2O_4\}\{HO_3PC(O)(CH_2\text{-}3\text{-}C_5NH_4)PO_3\}_2]\cdot 13H_2O$ (**1a**), which was insoluble in all common solvents. By using NaOH for pH adjustment, we were able to isolate a mixed sodium–guanidinium salt of polyanion **1**, $Na[C(NH_2)_3]_5[\{Mo^{VI}O_3\}_2\{Mo^{V}_2O_4\}\{HO_3P\text{–}C(O)(CH_2\text{-}3\text{-}C_5NH_4)PO_3\}_2]\cdot 10H_2O$ (**1b**), which was soluble in water. However, no single crystals of **1b** suitable for X-ray diffraction (XRD) could be obtained, and so the product was characterized by IR spectroscopy, multinuclear NMR spectroscopy, and elemental analysis. Polyanion **1** consists of two crystallographically unique Mo atoms in the asymmetric unit. Bond valence sum (BVS)[8] calculations showed that the oxidation states of Mo1 and Mo2 are +6 and +5, respectively (Table S1 in the Supporting Information, SI). The structure of polyanion **1** comprises a dinuclear $\{Mo^{V}_2O_4\}$ unit, being capped by a $Mo^{VI}O_6$ group on either side. This cationic $[\{Mo^{VI}O_3\}_2\{Mo^{V}_2O_4\}]^{2+}$ assembly is, in turn, stabilized by two tetra-deprotonated diphosphonate groups $\{HO_3PC(O)(CH_2\text{-}3\text{-}C_5NH_4)PO_3\}$ (Figure 1), resulting in an overall charge of 6– for polyanion **1**. The unsymmetrical deprotonation of the two P atoms in each diphosphonate moiety, and their subsequent unequal bonding (P1 connects to Mo^{VI} and Mo^{V}, whereas P2 connects to Mo^{VI}), renders the two P atoms chemically and magnetically inequivalent. Interestingly, the pyridine rings in polyanion **1** interact in a face-on fashion in the solid state, but somewhat offset, so that the sp^2-hybridized N atoms are located roughly above the center of the adjacent aromatic ring (Figure 1). The inter-ring distance of ca. 4 Å implies possible $\pi\cdots\pi$ interactions between the two rings, which are apparently too weak to enforce an eclipsed conformation of the rings.

Polyanion **2** was synthesized using reaction conditions similar to those for **1**, but with a 2:1 stochiometric ratio of $\{Mo^{V}_2O_4(H_2O)_6\}^{2+}$ to Risedronic acid, and also crystallized as a guanidinium salt, $[C(NH_2)_3]_6H_2[\{Mo^{VI}_2O_6\}_2\{Mo^{V}_2O_4\}\{O_3PC(O)(CH_2\text{-}3\text{-}C_5NH_4)PO_3\}_2]\cdot 10H_2O$ (**2a**). In analogy to **1a**, **2a** is

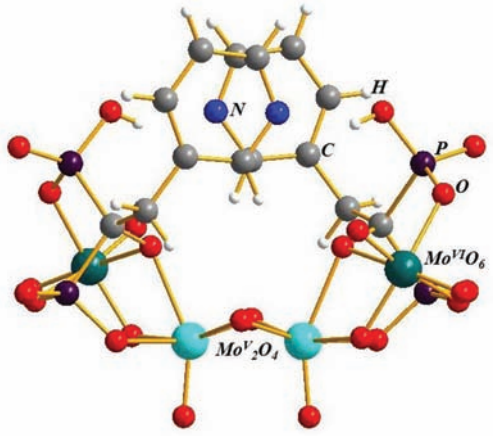

Figure 1. Ball-and-stick representation of **1**, viewed along the *a* axis.

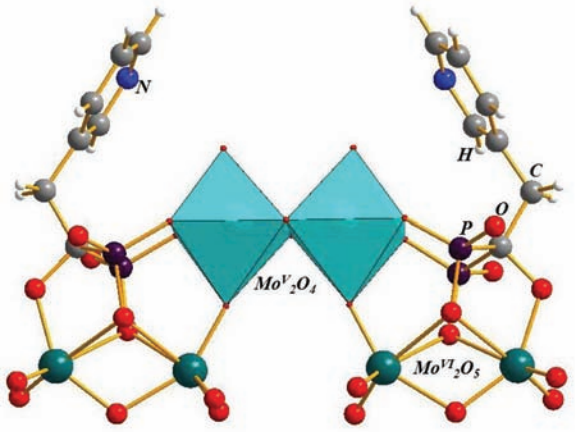

Figure 2. Combined ball-and-stick/polyhedral representation of **2**.

not soluble in all common solvents. Efforts to obtain water-soluble salts of polyanion **2** (including mixed alkali–guanidinium salts) were not successful. The asymmetric unit of polyanion **2** consists of a total of six Mo atoms, with Mo1, Mo2, Mo3, and Mo4 in oxidation state +6 and Mo5 and Mo6 in oxidation state +5, based on BVS calculations (Table S2 in the SI). The structure of polyanion **2** consists of an edge-shared $\{Mo^{V}_2O_4\}$ unit, which is corner-sharing with a face-shared $\{Mo^{VI}_2O_6\}$ unit on either side (Figure 2). This assembly is stabilized by two fully deprotonated diphosphonate moieties, one on each side, forming two P–O–Mo^{VI}, two P–O–Mo^{V}, and one C–O–Mo^{VI} bridge for each diphosphonate unit, resulting in an overall 8– charge for polyanion **2**. This type of structure has been previously reported by the groups of Wang and Dolbecq with 1-hydroxyethylidenediphosphonate (Etidronate)[7b] and 4-amino-1-hydroxybutyldiphosphonate (Alendronate).[7c,d] However, the alkyl groups of the diphosphonates in their structures point outward in the solid state, in contrast to the 3-pyridyl rings in **2**, which point toward each other.

Polyanion **3** was formed under reaction conditions similar to those of **1**, but at pH 6.4, and by using an 8 M NaOH solution for pH adjustment. Polyanion **3** was isolated as a mixed sodium–guanidinium salt, $Na_8[C(NH_2)_3]_4[\{Mo^{V}_2O_4(H_2O)\}_4\{O_3PC(O)(CH_2\text{-}3\text{-}C_5NH_4)PO_3\}_4]\cdot 8H_2O$ (**3a**). The asymmetric unit of polyanion **3** comprises two Mo atoms, both in the +5 oxidation

dx.doi.org/10.1021/ic201652h |*Inorg. Chem.* 2011, 50, 11667–11675

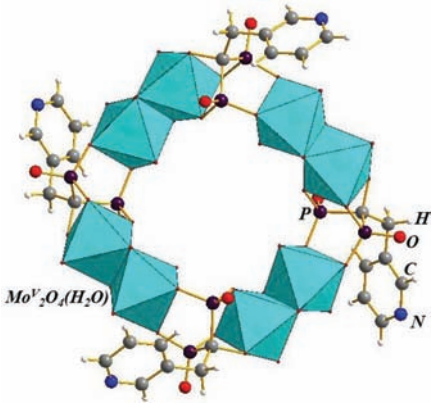

Figure 3. Combined ball-and-stick/polyhedral representation of **3**.

state (see BVS calculations; Table S3 in the SI). The structure of **3** is a cyclic assembly of four $\{Mo^{V}_2O_4(H_2O)\}$ units connected by four fully deprotonated Risedronate groups, forming a puckered ring (Figure 3). Such a structure has also been observed in our previously reported polyanion with F3-Etidronic acid[6] and very recently by the group of Mialane and Dolbecq with Alendronic acid.[7d] The most interesting aspect of such an assembly is the unique $\{Mo^{V}_2O_4(H_2O)\}$ unit, unlike the more common $\{Mo^{V}_2O_4\}$ unit, in addition to the enhanced solution stability of these cyclic compounds, compared to other cyclic polyanions obtained with Etidronic acid. We observed that compound **3a** was always contaminated with **1b** and/or Risedronic acid (see the Multinuclear NMR Studies section), with the exact ratio of **3a** and **1b** depending on the pH. At pH values lower than 6.6, **3a** crystallized along with some unknown compounds. When the pH of the reaction mixture was gradually increased, more **1b** was isolated, until at pH 7.6 pure **1b** was obtained. In spite of considerable efforts, no pure sample of **3a** could be isolated.

Weak Interactions and Crystal Packing. Extensive intra- and intermolecular hydrogen-bonded networks are observed in the solid state for **1a**−**3a** not only between guanidinium cations and polyanions but also between polyanions themselves. Such hydrogen bonding is prominent in these compounds because of the presence of donor atoms (N and C) and acceptor atoms (O) in both the cations and anions. Apart from the common weak interactions such as N−H···O and O−H···O, we also observed C−H···O interactions for some of the compounds. The latter types of weak hydrogen bonds are less frequently observed in POM chemistry.[9]

In compound **1a**, we can observe hydrogen bonding between adjacent polyanions along the *b* axis (Figure S1a in the SI) and also between the polyanions and guanidinium countercations in the *bc* plane (Figure S1b in the SI). This leads to the formation of an extensive two-dimensional array in the solid state. The anion−anion hydrogen bonding occurs between the terminal O atoms of the $\{Mo^{V}_2O_4\}$ unit and the H atoms of the sp^2-hybridized C atoms in the ortho position of the pyridine ring. This results in a linear arrangement of the polyanions in the solid state along the *b* axis (Figure S1a in the SI). On the other hand, the cation−anion interactions are not so simple, and extensive hydrogen bonding between the guanidinium cations and the polyanions generates an ABAB type of packing in the solid state as viewed along the *bc* plane (Figure S1b in the SI). A complete list of hydrogen-bonding interactions in **1a** is shown in Table S4 in the SI.

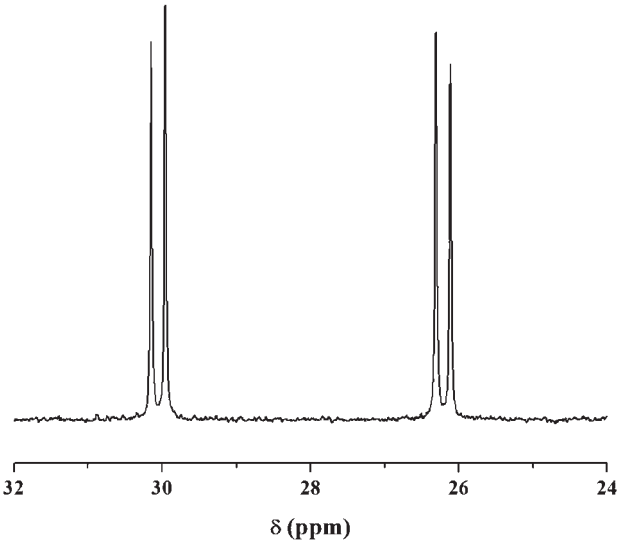

Figure 4. Solution $^{31}P\{^{1}H\}$ NMR spectrum of **1b** redissolved in D_2O at pH 7.4.

In the structure of compound **2a**, each polyanion forms intermolecular C−H···O hydrogen bonds with three other polyanions, two having an identical orientation with respect to the parent polyanion and one with an opposite orientation in the solid state (Figure S2a in the SI). This arrangement results in molecular layers of **2**, each formed by single rows of polyanions with alternating up−down orientation (Figure S2a, inset, in the SI). The guanidinium counterions occupy positions between the void spaces, engaging in extensive N−H···O interactions (Figure S2b in the SI). The absence of $\pi\cdots\pi$ interactions indicates that the packing is exclusively dominated by hydrogen bonding. The unusual orientation of the polyanions was the reason that no particular packing profile could be identified along any particular axis of **2a**. A complete list of hydrogen-bonding interactions in **2a** is given in Table S5 in the SI.

For compound **3a**, a packing similar to that for the previously reported isostructural polyanion based on F3-Etidronate is observed.[6] However, unlike for the fluorinated compound, the Na^+ countercations in **3** occupy the void spaces in addition to the positions between adjacent polyanions (Figure S3a,b in the SI). Such extensive Na···O interactions result in an AA-type packing mode along the *c* axis. The guanidinium countercations are located in the periphery of the polyanions and exhibit extensive hydrogen bonding with O atoms of Mo as well as P atoms (Figure S3c in the SI).

Multinuclear NMR Studies. We decided to perform multinuclear NMR studies on our compounds in order to investigate the solution stability of the respective polyanions. However, this was not possible for **2a** because of insufficient solubility. As **1a** is also insoluble in all common solvents, we worked with the soluble analogue **1b** (*vide supra*).

The structure of polyanion **1**, as described above, reveals that the two P atoms in each diphosphonate group are chemically and magnetically inequivalent (Figures 1 and S4 in the SI). We measured $^{31}P\{^{1}H\}$ NMR on **1b** redissolved in D_2O (15 mM solution), resulting in a pair of doublets at 30.1 and 26.2 ppm (Figure 4), in complete agreement with the solid-state structure. The ^{1}H NMR spectrum of **1** exhibits the following signals for the aromatic H atoms in the 2, 3, 4, and 6 positions (values in

dx.doi.org/10.1021/ic201652h |*Inorg. Chem.* 2011, 50, 11667–11675

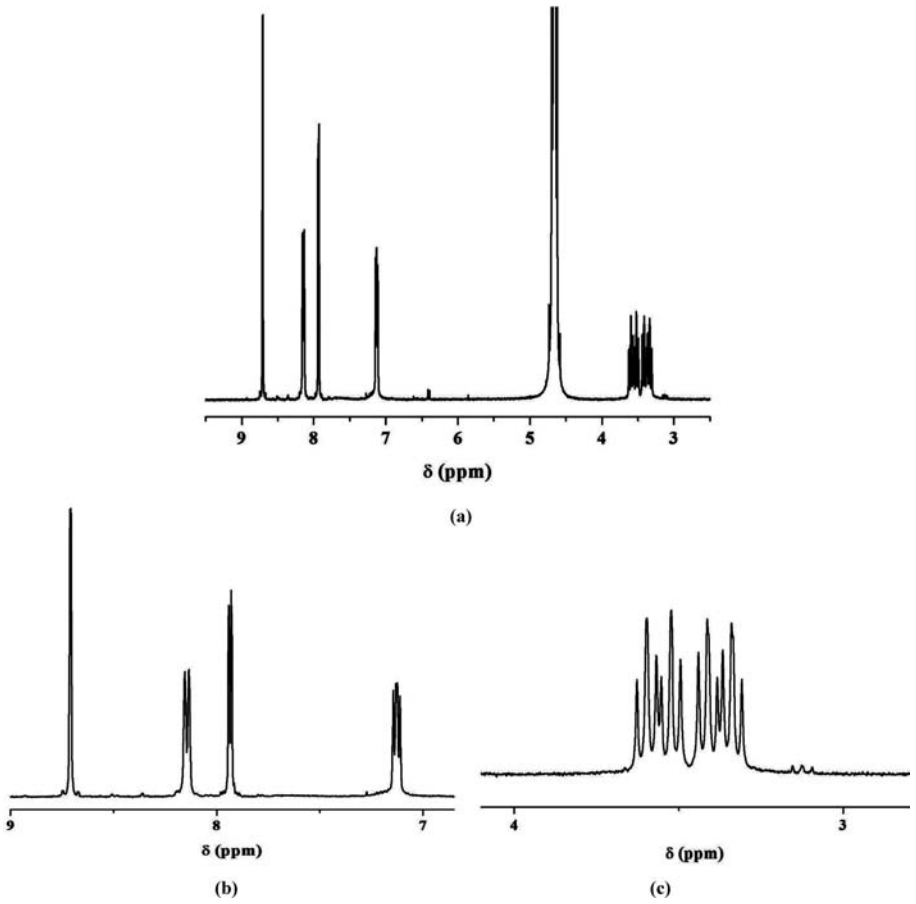

Figure 5. (a) Solution ^{1}H NMR spectrum of **1b** redissolved in D_2O: (b) aromatic region; (c) aliphatic region.

parentheses are for the corresponding H atoms of free Risedronate): 8.15 (8.26), 7.13 (7.26), 7.94 (7.86), and 8.71 (8.44), respectively (Figure 5b). These values show that the aromatic H atoms of **1** exhibit either upfield or downfield shifts, compared to free Risedronate, depending on the proximity or remoteness to the polyanion framework (Figure S4 in the SI). The H atoms located in the 4 and 6 positions show downfield shifts of 0.08 and 0.27 ppm, respectively, compared to those of the free diphosphonate. The H atoms in the 2 and 3 positions experience a small upfield shift of 0.13 ppm. An even larger effect in the ^{1}H NMR spectrum of polyanion **1** is observed for the two aliphatic H atoms of the diphosphonate moieties, which appear magnetically inequivalent in comparison to the ones of free Risedronic acid, exhibiting a triplet at 3.19 ppm. In **1**, these H atoms exhibit two doublets of triplets at 3.56 and 3.38 ppm, representing downfield shifts of 0.37 and 0.19 ppm, respectively, compared to free Risedronate (Figure 5c). The magnetic inequivalence of the methylene H atoms can be explained by the presence of a pseudochiral center at the adjacent aliphatic C atom (P−C−P) because of the structural and, hence, magnetic inequivalence of the P atoms in the diphosphonate groups of **1** (Figure S4 in the SI), which renders these two H atoms diasterotopic. A further explanation of this situation is provided in the Computational Studies on the Solution Behavior section.

The $^{31}P\{^{1}H\}$ NMR spectrum of **3a** redissolved in D_2O shows a pair of doublets at 19.3 and 30.5 ppm, which are similar to related polyanion structures based on other diphosphonates.[6,7d] The two P atoms in each diphosphonate moiety of **3** are magnetically inequivalent because of the different bonding patterns of the PO_3 groups to the Mo centers. While P1 has an equatorial−equatorial bonding mode, P2 has an axial−equatorial bonding mode.

As stated above, the synthesis of **3a** was complicated by the fact that impurities were always present. We observed the formation of mixtures of **3a** and **1b**, with the relative amount of impurities depending on the pH of the reaction solution. In order to study this equilibrium in solution, we decided to use $^{31}P\{^{1}H\}$ NMR for reactions performed between pH 6.0 and 7.6, modified in 0.2 units. We observed that in the range pH 6.0−6.4 the product mixture contained several compounds including polyanion **3** and free Risedronate. Upon increasing the pH to 6.6, the presence of only polyanion **3** and Risedronate was observed. A further increase to pH 6.8 resulted also in polyanion **1** in the product mixture. When the pH was increased to 7.0, a decrease in the amount of **3** and Risedronate in the product mixture was observed (Figure 6). This trend continued until pH 7.4, and the pure polyanion **1** could be isolated as a mixed sodium−guanidinium salt at pH 7.6. No pure crystalline sample of **3a** could be obtained at pH 6.6 because of the continuous coprecipitation of Risedronate.

Computational Studies on the Solution Behavior. Further insight into the structure of polyanions **1** and **3** in solution was provided by means of density functional theory (DFT) calculations employing the Amsterdam density functional code (ADF 2010[10]), with relativistic corrections (ZORA formalism[11] and spin−orbit coupling) and the solvent medium (COSMO method[12]) taken into account. Full geometry optimizations (using the GGA BP86 functional[13a,b] for **1** and the BP86-D3 functional[13c] for **3**) were

dx.doi.org/10.1021/ic201652h |*Inorg. Chem.* 2011, 50, 11667–11675

carried out, followed by ^{1}H and ^{31}P NMR chemical shift calculations employing the model SAOP potential.[13d,14] Chemical shifts have been computed with respect to tetramethylsilane (TMS; ^{1}H NMR) and phosphoric acid (^{31}P NMR).

Considering the experimental fact that the ^{1}H and ^{31}P NMR spectra of **1** were obtained for its soluble sodium−guanidinium salt **1b**, as well as the recently reported[14] finding that the counterion shell can play a significant role in the POM solution state and composition, we simulated the bare polyanion, as well as derivatives comprising two, four, or six Na^{+} counterions. Here we discuss two of the species modeled in solution: the bare polyanion, which we denote as $[\mathbf{1}]^{8-}$, and an ion-pair assembly involving four Na atoms, denoted as $[Na_4\mathbf{1}]^{4-}$, in terms of their

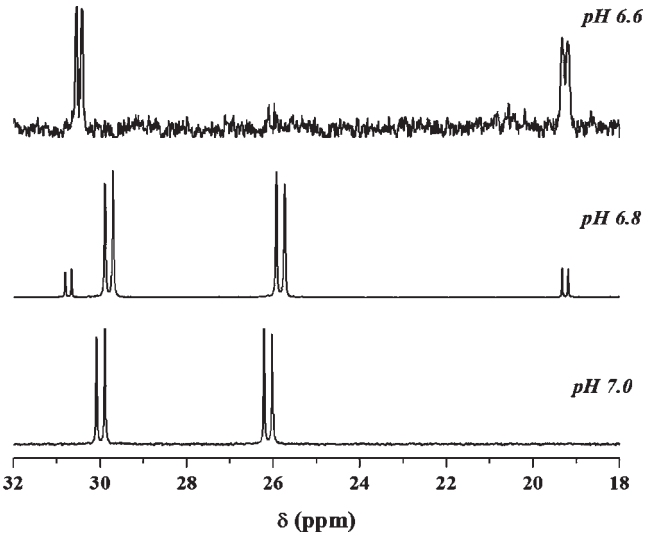

Figure 6. Solution $^{31}P\{^{1}H\}$ NMR spectra showing the pH-dependent formation of polyanions **1** and **3** (see the text for details).

comparison to the crystal structure of **1** and to the solution NMR data measured for **1b**. More detailed comparisons including all simulated structures can be found in the SI.

Our calculations confirm that polyanion **1** stays intact in solution. Its characteristic basketlike shape is well preserved in both $[\mathbf{1}]^{8-}$ and $[Na_4\mathbf{1}]^{4-}$ model species, but is calculated to be slightly more open than that in the solid state (e.g., the distance between the two Mo^{VI} centers is 8.35 Å in $[\mathbf{1}]^{8-}$ and 8.49 Å in $[Na_4\mathbf{1}]^{4-}$ versus 8.12 Å in the crystal structure of **1**). Interestingly, during geometry optimization of $[\mathbf{1}]^{8-}$, significant rotation of the two pyridine groups takes place and is associated with a change of the dihedral angle between the pyridine plane and the plane defined by the two adjacent aliphatic C atoms (Figure 7) from 274.6°, reflecting the crystal structure, to 218.6° in the minimized solution structure (movie S1 in the SI). The pincer-like stacking pattern of the pyridine moieties is preserved in general, but the orientation of the aromatic rings with respect to the rest of the molecule is alternated in such a way that the distance of the two N atoms in $[\mathbf{1}]^{8-}$ is almost twice as large as that in **1**, whereas that of the aromatic C atoms in the para position is ∼1.5 times shorter (cf. Figures 1 and 7a). In contrast, the inclusion of Na^{+} ions in the vicinity of polyanion **1** when modeling its solution state stabilizes almost the same orientation of the pyridine rings as the one characterizing the crystal structure (Figures 1 and 7b). For instance, the calculations predict 274.2° for the above-mentioned dihedral angle, 3.97 Å for the distances of the N centers, and 7.44 Å for the *p*-C atoms in $[Na_4\mathbf{1}]^{4-}$, versus 274.6°, 3.19 Å, and 6.03 Å, as determined respectively in the solid state. The slightly increased distance between the pincerlike oriented organic parts in $[Na_4\mathbf{1}]^{4-}$ is due to the electrostatically enhanced penetration of two Na^{+} ions between the aromatic rings and the nearest-lying phosphonate and $Mo^{VI}O_6$ moieties of the polyanion.

The outlined differences between the model structures of $[\mathbf{1}]^{8-}$ and $[Na_4\mathbf{1}]^{4-}$ are reflected in the considerably different ^{1}H

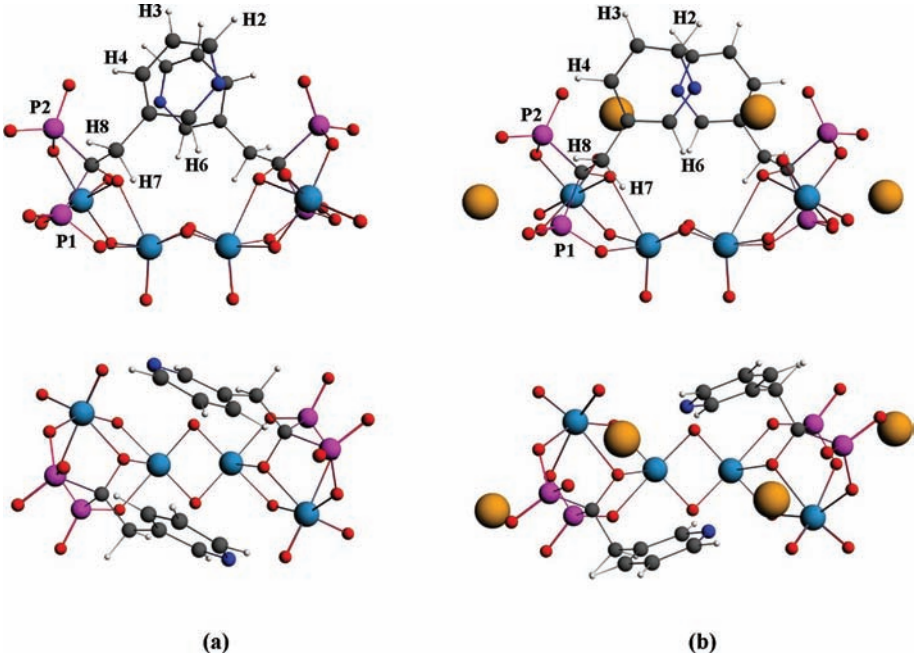

Figure 7. Ball-and-stick representations of (a) $[\mathbf{1}]^{8-}$ and (b) $[Na_4\mathbf{1}]^{4-}$, as modeled by DFT calculations in aqueous solution (geometries optimized at the BP86/ZORA/TZ2P/COSMO level), with annotation for the inequivalent H and P atoms. Side (up) and top (down) views of the model structures. Color legend: Mo, light blue; P, pink; O, red; N, dark blue; C, gray; H, white; Na, yellow.

dx.doi.org/10.1021/ic201652h |*Inorg. Chem.* 2011, 50, 11667–11675

Table 1. ^{1}H and ^{31}P NMR Chemical Shifts, δ, As Calculated for $[\mathbf{1}]^{8-}$ and $[Na_4\mathbf{1}]^{4-}$ Model Structures and As Measured Experimentally for 1b[a]

			calculated δ [ppm]		deviation [ppm]	
nucleus type	nucleus notation	experimental δ [ppm]	$[\mathbf{1}]^{8-}$	$Na_4[\mathbf{1}]^{4-}$	$[\mathbf{1}]^{8-}$	$Na_4[\mathbf{1}]^{4-}$
aliphatic H	**H8**	**3.38**	2.63	**3.08**	−0.75	**−0.3**
	H7	**3.56**	4.22	**3.84**	0.66	**0.28**
aromatic H	**H3**	**7.13**	6.61	**7.12**	−0.52	**−0.01**
	H4	**7.94**	11.51	**8.03**	3.57	**0.09**
	H2	**8.15**	8.07	**8.08**	−0.08	**−0.07**
	H6	**8.71**	9.07	**9.53**	0.36	**0.82**
$Mo^{V,VI}$-capping P	**P1**	**30.1**	32.12	**31.92**	2.02	**1.82**
Mo^{VI}-capping P	**P2**	**26.2**	25.86	**25.8**	−0.34	**−0.4**
MAD[b] for ^{1}H NMR [ppm]					0.99	**0.26**
MAD[b] for ^{31}P NMR [ppm]					1.18	**1.11**

[a] NMR calculations on optimized geometries in water (SAOP/ZORA + spin orbit/AE-TZP/COSMO//BP86/ZORA/AE-TZ2P/COSMO). TMS and 85% phosphoric acid were used as ^{1}H and ^{31}P NMR reference samples, respectively. The deviation, $\delta_{CALC} - \delta_{EXP}$, is also given. [b] Mean absolute deviation (MAD) defined as the mean absolute value of the deviation calculated from the experimental chemical shifts, $\delta_{CALC} - \delta_{EXP}$.

and ^{31}P NMR spectra derived from the calculations (Table 1). The computed chemical shifts, δ_{CALC}, for the magnetically inequivalent aliphatic protons, H7 and H8, show good agreement with the experimental data, δ_{EXP}, when the ion pair model $[Na_4\mathbf{1}]^{4-}$ is considered. In this case, δ_{CALC} is overestimated for H7 and underestimated for H8 by only 0.3 ppm. In the case of the bare anion $[\mathbf{1}]^{8-}$, the deviation from δ_{EXP} increases more than twice following the same trend (downfield shift for H7 and upfield shift for H8). The stronger deshielding of H7 in $[\mathbf{1}]^{8-}$ can be explained by the proximity of these protons to the O atoms bridging the two Mo^{V} centers [H7···$O_b(Mo^{V,V})$ = 2.49 Å], close enough for the formation of intramolecular hydrogen bonds. In $[Na_4\mathbf{1}]^{4-}$, this distance is increased to 2.84 Å and, therefore, H7 experiences the deshielding effect of $O_b(Mo^{V,V})$ to a much smaller extent.

The experimental chemical shifts of the aromatic protons denoted as H2, H3, and H4 are nicely reproduced by the calculations considering the ion-pair model $[Na_4\mathbf{1}]^{4-}$, with the deviation being less than 0.1 ppm (Table 1). In contrast, when the bare polyanion $[\mathbf{1}]^{8-}$ is subjected to NMR calculations, a very strong deshielding by 3.6 ppm is computed for H4 because of enhanced intramolecular hydrogen bonding to a terminal O atom of the nearest-lying phosphonate group (H4···O_t = 1.88 Å), arising from the staggered orientation of the pyridine rings (Figure 7). As for $[Na_4\mathbf{1}]^{4-}$, the H4···O_t distance is more than 1 Å larger because of the presence of a competing electrostatic interaction between the terminal O center and a Na^+ ion (Na^+···O = 2.34 Å). As a result of charge redistribution (Table S13 in the SI), the NMR shielding of H3 in $[\mathbf{1}]^{8-}$ is increased, which, in turn, leads to an underestimation of δ_{CALC} by more than 0.5 ppm relative to the respective δ_{EXP} value (Table 1). The only protons for which the $[\mathbf{1}]^{8-}$ model outperforms the $[Na_4\mathbf{1}]^{4-}$ model in terms of correlation between δ_{CALC} and δ_{EXP} are those denoted as H6, whose resonance appears most downfield in the experimental spectrum (δ_{EXP} = 8.71 ppm) because of the adjacency of the electronegative N atoms and the $\{Mo^{V}_2O_4\}$ moiety. Our calculations predict larger chemical shifts for both model species, with a deviation of 0.36 and 0.82 ppm for the bare anion and the ion pair, respectively. We attribute the stronger deshielding of H6 in the models for **1b** to the proximity of these protons to the $O_b(Mo^{V,V})$ centers, allowing for weak intramolecular interactions. The shorter H6···$O_b(Mo^{V,V})$ distance (cf. 2.59 Å in $[Na_4\mathbf{1}]^{4-}$ vs 3.1 Å in $[\mathbf{1}]^{8-}$), as well as the proper mutual orientation of these H and O atoms in $[Na_4\mathbf{1}]^{4-}$ (Figure 7b), explains the larger chemical shift of H6 in the case of the ion-pair model species.

According to the calculations on $[\mathbf{1}]^{8-}$ and $[Na_4\mathbf{1}]^{4-}$, the ^{31}P NMR spectrum of polyanion **1** seems to be affected more by the presence and number of Na^+ counterions than by the changes in the orientation of the organic moieties. This concerns especially the atom P1 capping Mo^{V} and Mo^{VI} centers (Figure 7), for which the calculated chemical shift in the case of $[\mathbf{1}]^{8-}$ is overestimated by 2 ppm (δ_{CALC} = 32.12 ppm) relative to the corresponding experimental value of 30.1 ppm. The presence of four Na^+ ions in the vicinity of the polyanion leads to a slight increase of the shielding of P1 and eventually to a slightly improved agreement with δ_{EXP} (δ_{CALC} = 31.92 ppm). Concerning the atom P2 capping a Mo^{VI} center (Figure 7), δ_{CALC} for both $[Na_4\mathbf{1}]^{4-}$ and $[\mathbf{1}]^{8-}$ is virtually the same and only ∼0.4 ppm smaller than the respective experimental data (cf. δ_{CALC} = 25.8 ppm vs δ_{EXP} = 26.2 ppm; Table 1).

It is worth noting that the inclusion of two more Na ions (six Na^+ ions in total; Figure S7b in the SI) in our model leads to further deshielding of P1 and further shielding of P2 and, consequently, to larger deviations (2.9 and −4.1 ppm, respectively) from the experimental ^{31}P NMR spectrum of **1b** (Table S6 in the SI).

In conclusion, the comparison between calculated and experimental data for the ^{1}H and ^{31}P NMR spectra of **1b** clearly shows that the solvated polyanion exists in the form of an ion pair involving four Na ions rather than a bare anion with a dynamic solvent shell. The $[Na_4\mathbf{1}]^{4-}$ model proposed by the calculations represents very well the composition and structure of **1b** in solution because it reproduces the experimental chemical shifts with only a minor difference (mean absolute deviation of ∼0.3 ppm for ^{1}H NMR and ∼1 ppm for ^{31}P NMR). As a general trend, our calculations show that, on the one hand, the presence of counterions surrounding **1** affects the orientation of the organic moieties with respect to the rest of the polyanion, which, in turn, is associated with stronger or weaker intramolecular hydrogen bonding and, hence, is crucial for the ^{1}H NMR properties. On the other hand, the exact number and position of the Na^+ ions

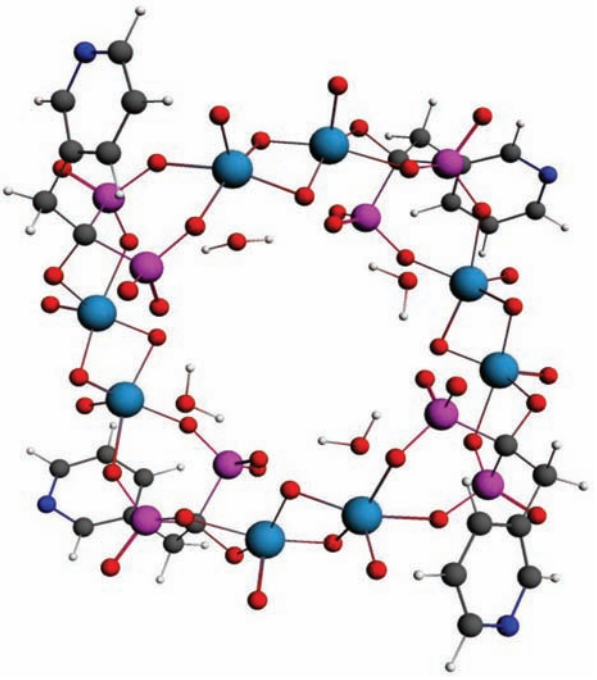

Figure 8. Ball-and-stick representation (top view) of the cyclic tetranuclear assembly of polyanion **3**, as modeled by DFT calculations in aqueous solution (geometry optimized at the BP86-D3/ZORA/TZ2P/COSMO level). The color legend is the same as that in Figure 7.

influences considerably the shielding of the phosphorus nuclei and, accordingly, the ^{31}P NMR spectrum of **1b**.

Our calculations regarding polyanion **3** show that its characteristic structure, a cyclic tetramer comprising four $\{Mo^{V}_2O_4(H_2O)\}$ units, is well-preserved in aqueous solution (Figure 8). In comparison to the crystal structure, however, the optimized geometry in water (movie S2 in the SI) is contracted and slightly distorted in the plane defined by the crystallographic axes *a* and *b*. In the solid state, as shown by XRD, the opposite $Mo^{V}-Mo^{V}$ pairs are equidistant from each other (Figure 3). In solution, according to the calculations, the distance between opposite $Mo^{V}-Mo^{V}$ pairs for one of the two mutually perpendicular sets has shortened by 0.3 Å and for the other by 0.22 Å. This result is in agreement with previously reported[15] computational findings that polyanions contract upon hydration. In the simulated solution structure of **3**, each of the four H_2O molecules remains in close proximity to its corresponding Mo center within the four $Mo^{V}-Mo^{V}$ pairs (calculated distance $Mo^{V}-OH_2$ ~2.35 Å). Seven of all eight hydroxylic protons form hydrogen bonds with four terminal O atoms, each belonging to a different PO_3 group capping a single Mo^{V} center (four hydrogen bonds in the range of 1.73−1.79 Å and the remaining three in the range of 1.82−1.86 Å).

The computed NMR chemical shifts for the two inequivalent P nuclei in the model structure, as depicted in Figure 8, match well the experimental ^{31}P NMR spectrum of polyanion **3**. For the P nuclei capping a single Mo^{V} center, we obtained δ_{CALC} = 19.38 ppm, which differs by only 0.11 ppm from the measured δ_{EXP} = 19.27 ppm. For the P nuclei bridging two Mo^{V} centers from two adjacent $\{Mo^{V}_2O_4(H_2O)\}$ units, we expected to exhibit a downfield shift (i.e., larger δ value) because it is connected via two bridging O atoms (with a deshielding effect) to the respective Mo atoms. For these P nuclei, the computed chemical shift was underestimated by ~1.9 ppm relative to the experimental value (cf. δ_{CALC} = 28.61 ppm vs δ_{EXP} = 30.49 ppm). On the basis of this comparison, we conclude that in solution polyanion **3** is present as a cyclic, tetrameric assembly and four H_2O molecules that engage in hydrogen bonding with the phosphonate groups capping a single Mo^{V} center.

CONCLUSIONS

We have successfully incorporated Risedronic acid into polyoxomolybdates by one-pot reactions of the dinuclear dication $\{Mo^{V}_2O_4(H_2O)_6\}^{2+}$ with the free acid. Employing a simple synthetic approach and by systematically varying the reaction parameters such as the pH and ratio of reagents, we isolated the first three examples of risedronate-containing polyoxomolybdates, $[\{Mo^{VI}O_3\}_2\{Mo^{V}_2O_4\}\{HO_3PC(O)(CH_2\text{-}3\text{-}C_5NH_4)PO_3\}_2]^{6-}$ (**1**), $[\{Mo^{VI}_2O_6\}_2\{Mo^{V}_2O_4\}\{O_3PC(O)(CH_2\text{-}3\text{-}C_5NH_4)\text{-}PO_3\}_2]^{8-}$ (**2**), and $[\{Mo^{V}_2O_4(H_2O)\}_4\{O_3PC(O)(CH_2\text{-}3\text{-}C_5NH_4)PO_3\}_4]^{12-}$ (**3**). Polyanion **1** is structurally unprecedented, whereas the structures of **2** and **3** are known for other diphosphonates. This work revealed that a subtle modification of the pH of the reaction solution can result in completely different polyanion structures. A detailed solution NMR speciation study shed further light on the formation equilibria of this class of polyanions. Additional computational studies performed on **1** and **3** indicated the stability of the structures in solution, but with slight rearrangements of the aromatic rings compared to the solid state. Also, the formation of an ion pair in solution is proposed for polyanion **1**, resulting in a better correlation with experimental NMR data. For **3** in solution, the bare polyanion itself was observed to give a satisfactorily close match with experimentally observed NMR chemical shifts.

In essence, our experimental work suggests that in diphosphonate-containing polyoxomolybdate chemistry pH changes have more dramatic effects on the polyanion structure than changes in the diphosphonate hetero groups. In addition, our computational studies suggest that the role of countercations must not be underestimated because of the formation of ion pairs in solution. The above implies that most likely some more novel structural types of diphosphonate-containing polyoxomolybdates will be discovered in the near future. We have also demonstrated that computational studies are nowadays at such an advanced level that they should be more routinely used, especially for a better understanding of the solution behavior of polyanions. Such studies are even more important in cases where solution NMR is not possible, for example, because of the lack of solubility and/or the paramagnetic nature of the target compound.

Currently, we are investigating the reactivity of other isomers of pyridine-based 1-hydroxyethylidenediphosphonates with molybdates, in order to explore a possible influence of the position of the N atom on the resulting polyanion structure and the orientation of the pyridyl rings to each other.

EXPERIMENTAL SECTION

Single-Crystal X-ray Diffraction. Single crystals of **1a** and **3a** were mounted on a Hampton cryoloop, whereas **2a** was mounted on a glass fiber for indexing and intensity data collection at 173 K (**1a** and **3a**) and 296 K (**2a**) on a Bruker SMART APEX II CCD single-crystal diffractometer using Mo Kα radiation (λ = 0.710 73 Å). Direct methods were used to solve the structures and to locate the heavy atoms (*SHELXS97*), and the remaining atoms were found from successive difference maps (*SHELXL97*).[16] Routine Lorentz and polarization

dx.doi.org/10.1021/ic201652h |*Inorg. Chem.* 2011, 50, 11667–11675

Table 2. Crystal Data and Structure Refinement Parameters for Compounds 1a, 2a, and 3a

	1a	2a	3a
empirical formula	$Mo_4P_4C_{19}N_{17}O_{37}H_{71}$	$Mo_6P_4C_{20}N_{20}O_{40}H_{70}$	$Mo_8P_8C_{32}N_{16}O_{56}H_{64}Na_8$
molar mass (g mol^{-1})	1637.57	1930.48	2776.26
cryst syst	monoclinic	triclinic	tetragonal
space group	$C2/c$	$P\bar{1}$	$P4/n$
a (Å)	18.216(3)	11.2994(4)	25.3368(11)
b (Å)	10.638(3)	12.5679(4)	25.3368(11)
c (Å)	28.070(6)	19.8205(6)	8.0896(4)
α (deg)	90	81.723(2)	90
β (deg)	90.605(14)	79.307(2)	90
γ (deg)	90	78.468(2)	90
volume (Å^3)	5439(2)	2693.25(15)	5193.1(4)
Z	4	2	2
temp (K)	173(2)	296(2)	173(2)
ρ_{calcd} (g cm^{-3})	2.000	2.380	1.775
abs coeff	1.135	1.604	1.184
GOF	1.034	1.025	1.010
R1[a] $[I > 2\sigma(I)]$	0.0238	0.0543	0.0499
wR2[a]	0.0668	0.1579	0.1771

[a] $R1 = \Sigma||F_o| - |F_c||/\Sigma|F_o|$. $wR2 = \{\Sigma[w(F_o^2 - F_c^2)]/\Sigma[w(F_o^2)^2]\}^{1/2}$.

corrections were applied, and an absorption correction was performed using the *SADABS* program.[17] For **1a** and **3a**, all non-H atoms were refined anisotropically, whereas for **2a**, only the Mo and P atoms were refined anisotropically. For **1a**−**3a** the hydrogens of all the C and N atoms were added in calculated positions and refined using a riding model, and in **1a** the crystal water hydrogens were found directly by XRD. Crystallographic data are summarized in Table 2.

Synthesis. *Risedronic acid.* We have slightly modified the published synthesis procedure of Risedronic acid.[18] To 2.0 g (11.5 mmol) of 3-pyridyl acetic acid hydrochloride, taken in a 100-mL two-necked flask equipped with a reflux condenser, was added 3.6 g (43.8 mmol) of phosphorus acid and 12.0 g (86.3 mmol) of *p*-nitrophenol. The mixture was heated to 90 °C for a period of approximately 2 h until all of the solids had melted, forming a thick suspension. Then 7.0 g of phosphorus trichloride was added to this suspension, and the resulting mixture was kept at 90 °C for an additional period of 6 h, after which a yellow, gel-like material was formed. This mixture was allowed to cool to room temperature; 20 mL of water was then added dropwise, and the mixture was kept refluxing for 12 h (overnight). Then the mixture was again allowed to cool to room temperature, 15 mL of methanol was then added, and the precipitated product was kept stirring at 0−5 °C for an additional period of 2 h. The white, amorphous product obtained was filtered under suction and washed with methanol (yield 2.62 g, 81.4%). ^{1}H NMR (400 MHz, D_2O/NH_3): δ 3.19 (t, $^3J_{HP}$ = 12.1 Hz, 2H), 7.20 (dd, $^2J_{HH}$ = 8.2 and 5.5 Hz, 1H), 7.78 (d, $^2J_{HH}$ = 5.5 Hz, 1H), 8.19 (dd, $^2J_{HH}$ = 4.0 and 1.6 Hz, 1H), 8.37 (s, 1H). ^{31}P NMR (400 MHz, D_2O/NH_3): δ 18.1.

$[Mo^V_2O_4(H_2O)_6]^{2+}$. The synthesis was also performed according to the literature procedure.[5c] To a suspension of MoO_3 (2.3 g, 16 mmol) in 4 M HCl (80 mL) was added $N_2H_4 \cdot H_2O$ (210 μL, 4.29 mmol). The solution changed color slowly from deep yellow to dark red during heating at 80 °C for 3 h. The solution was then left to cool to room temperature and used subsequently for further reactions.

$[C(NH_2)_3]_5H[\{Mo^{VI}O_3\}_2\{Mo^V_2O_4\}\{HO_3PC(O)(CH_2\text{-}3\text{-}C_5NH_4)PO_3\}_2]\cdot 13H_2O$ (**1a**). To 5 mL of a $[Mo_2O_4(H_2O)_6]^{2+}$ solution in 4 M HCl (0.5 mmol) was added 0.15 g (0.5 mmol) of Risedronic acid. The pH of the solution was then adjusted to 7.7 with a 33% aqueous ammonia solution, and then guanidinium chloride (1.0 g, 10.4 mmol) was added to the above mixture, which was kept stirring at room temperature for 15 min. The precipitate formed was filtered off, and the resulting red filtrate was left for slow evaporation in an open vial. After 3 days, red block-shaped crystals of **1a** were formed. Yield: 0.19 g (46% based on Mo). Elem anal. Calcd for **1a**: Mo, 23.44; P, 7.57; C, 13.94; N, 14.54; H, 4.37. Found: Mo, 23.14; P, 7.48; C, 13.58; N, 14.98; H, 3.96. IR: 1658(s), 1581(w), 1569(w), 1444(sh), 1406(m), 1162(sh), 1131(s), 1070(s), 1051(s), 1032(w), 991(s), 921(s), 803(w), 746(m).

$Na[C(NH_2)_3]_5[\{Mo^V_2O_4\}_2\{Mo^{VI}O_3\}_2\{HO_3P{-}C(O)(CH_2\text{-}3\text{-}C_5NH_4)PO_3\}_2]\cdot 10H_2O$ (**1b**). **1b** was synthesized using the same procedure as that for **1a**, but the pH was adjusted with 8 M NaOH instead. Yield: 0.16 g (40% based on Mo). Elem anal. Calcd for **1a**: Mo, 23.06; P, 7.45; C, 13.72; N, 14.31; H, 3.88, Na 2.76. Found: Mo, 22.52; P, 7.33; C, 14.39; N, 15.08; H, 3.60; Na, 2.87. IR: 1665(s), 1587(sh), 1581(w), 1482(w), 1429(m), 1143(sh), 1116(s), 1055(s), 1024(s), 960(s), 921(sh), 849(w), 795(w), 742(m). ^{1}H NMR (400 MHz, D_2O): δ 3.38, 3.56 (dt, $^2J_{HH}$ = 29.3 Hz, $^3J_{HP}$ = 11.9 Hz, 1H), 7.94 (d, $^2J_{HH}$ = 8 Hz, 1H), 7.13 (dd, $^2J_{HH}$ = 2.8 and 8 Hz, 1H), 8.15 (d, $^2J_{HH}$ = 8 Hz, 1H), 8.71 (s, 1H). ^{31}P{^{1}H} NMR: δ 30.1, 26.2 (d, $^2J_{PP}$ = 29.7 Hz).

$[C(NH_2)_3]_6H_2[\{Mo^{VI}_2O_6\}_2\{Mo^V_2O_4\}\{O_3PC(O)(CH_2\text{-}3\text{-}C_5NH_4)PO_3\}_2]\cdot 10H_2O$ (**2a**). To 5 mL of a $[Mo_2O_4(H_2O)_6]^{2+}$ solution in 4 M HCl (0.5 mmol) was added 0.075 g (0.25 mmol) of Risedronic acid. The pH of the solution was then adjusted to 7.4 with a 33% aqueous ammonia solution, and then guanidinium chloride (1.0 g, 10.4 mmol) was added to the above mixture, which was kept stirring at room temperature for 15 min. The precipitate formed was filtered off, and the resulting pale-yellowish-red filtrate was left for slow evaporation in an open vial. After 5 days, red block-shaped crystals of **2a** were formed. Yield: 0.02 g (5.8% based on Mo). Elem anal. Calcd for **2a**: Mo, 29.82; P, 6.42; C, 12.44; N, 14.51; H, 3.65. Found: Mo, 30.04; P, 6.03; C, 11.95; N, 14.37; H, 3.21. IR: 1647(s), 1577(w), 1554(w), 1540(sh), 1466(w), 1439(m), 1405(sh), 1363(w), 1146(s), 1114(s), 1068(s), 1035(s), 957(w), 924(s), 869(m), 823(m), 707(m), 670(m).

$Na_8[C(NH_2)_3]_4[\{Mo^V_2O_4(H_2O)\}_4\{O_3PC(O)(CH_2\text{-}3\text{-}C_5NH_4)PO_3\}_4]\cdot 8H_2O$ (**3a**). To a solution of 0.1 M $[Mo_2O_4(H_2O)_6]^{2+}$ in 4 M HCl (5 mL, 0.5 mmol) was added 0.15 g of Risedronic acid (0.5 mmol). The pH of the solution was then adjusted to 6.7 with a 8 M NaOH solution. Guanidinium chloride (1.0 g, 10.4 mmol) was added to the above

dx.doi.org/10.1021/ic201652h |*Inorg. Chem.* 2011, 50, 11667–11675

mixture, which was stirred at room temperature for 15 min, and then the precipitate was filtered off. The resulting filtrate was left for 3 days in an open vial for slow evaporation, leading to yellowish-red needle-shaped crystals of **3a** together with deep-red blocks of **1b**. $^{31}P\{^{1}H\}$ NMR (400 MHz, D_2O): δ 30.5, 19.3 (d, $^{2}J_{PP}$ = 19.2 Hz).

■ ASSOCIATED CONTENT

Supporting Information. X-ray crystallographic data in CIF format, tables for BVS calculations (Tables S1−S3), hydrogen-bonding interactions (Tables S4 and S5), and computational data for polyanions **1** (Tables S6−S13) and **3** (Tables S14 and S15), figures for the packing profile (Figures S1−S3), NMR-active fragment of polyanion **1** (Figure S4), IR spectra (Figure S5), and computed geometries of polyanions **1** and **3** in solution (Figures S6−S8), movies for **1** and **3** (movies S1 and S2), showing their geometry optimization in solution, and optimized Cartesian coordinates of **1** and **3**. This material is available free of charge via the Internet at http://pubs.acs.org.

■ AUTHOR INFORMATION

Corresponding Author
*E-mail: u.kortz@jacobs-university.de.

■ ACKNOWLEDGMENT

We thank Jacobs University and the Nanomolecular Science Research Center for research support. Figures 1−3 were generated using *Diamond*, version 3.2 (copyright Crystal Impact GbR).

■ REFERENCES

(1) (a) Bartl, R.; Frisch, B.; Tresckow, E.; Bartl, C. *Bisphosphonates in Medical Practice*; Springer-Verlag: Berlin, 2007. (b) Fleisch, H. *Bisphosphonates in Bone Diseases: From the Laboratory to the Patient*; Academic Press: San Diego, CA, 2000. (c) Francis, M. D.; Valent, D. J. *J. Musculoskelet. Neuronal. Interact.* **2007**, *7*, 2. (d) Fleisch, H.; Bonjour, J. P. *N. Engl. J. Med.* **1973**, *289*, 1419. (e) Dunn, C. J.; Goa, K. L. *Drugs* **2001**, *61*, 685. (f) Major, P. *The Oncologist* **2002**, *7*, 481.

(2) (a) Pope, M. T. *Heteropoly and Isopoly Oxometalates*; Springer-Verlag: Berlin, 1983. (b) Hill, C. L.; Prosser-McCartha, C. M. *Coord. Chem. Rev.* **1995**, *143*, 407. (c) Pope, M. T.; Müller, A. *Angew. Chem., Int. Ed. Engl.* **1991**, *30*, 34. (d) *Chem. Rev.* **1998**, *98* (Special Issue on Polyoxometalates; Hill, C. L., Ed.). (e) Müller, A.; Roy, S. *Coord. Chem. Rev.* **2003**, *245*, 153. (f) Coronado, E.; Day, P. *Chem. Rev.* **2004**, *104*, 5419. (g) Cronin, L. In *Comprehensive Coordination Chemistry II*; McCleverty, J. A., Meyer, T. J., Eds.; Elsevier: Amsterdam, The Netherlands, 2004; Vol. 7, pp 1−57. (h) Hill, C. L. *J. Mol. Catal. A: Chem.* **2007**, *262*, 2. (i) Kortz, U.; Müller, A.; van Slageren, J.; Schnack, J.; Dalal, N. S.; Dressel, M. *Coord. Chem. Rev.* **2009**, *253*, 2315. (j) *Eur. J. Inorg. Chem.* **2009**, *34* (Issue dedicated to Polyoxometalates; Kortz, U., Guest Ed.).

(3) Rhule, J. T.; Hill, C. L.; Judd, D. A. *Chem. Rev.* **1998**, *98*, 327.

(4) (a) Kortz, U.; Jameson, G. B.; Pope, M. T. *J. Am. Chem. Soc.* **1994**, *116*, 2659. (b) Sarafianos, S. G.; Kortz, U.; Pope, M. T.; Modak, M. J. *Biochem. J.* **1996**, *319*, 619. (c) Kortz, U.; Pope, M. T. *Inorg. Chem.* **1994**, *33*, 5643. (d) Kortz, U.; Pope, M. T. *Inorg. Chem.* **1995**, *34*, 2160. (e) Kortz, U.; Pope, M. T. *Inorg. Chem.* **1995**, *34*, 3848. (f) Kortz, U. *Inorg. Chem.* **2000**, *39*, 625.

(5) (a) Peloux, P.; Dolbecq, A.; Mialane, P.; Marrot, J.; Sécheresse, F. *Dalton Trans.* **2004**, 1259. (b) Dolbecq, A.; Lisnard, L.; Mialane, P.; Marrot, J.; Benard, M.; Rohmer, M. M.; Sécheresse, F. *Inorg. Chem.* **2006**, *45*, 5898. (c) Compain, J. D.; Dolbecq, A.; Marrot, J.; Mialane, P.; Sécheresse, F. *C. R. Chim.* **2010**, *13*, 329.

(6) Banerjee, A.; Bassil, B. S.; Röschenthaler, G.-V.; Kortz., U. *Eur. J. Inorg. Chem.* **2010**, 3915.

(7) (a) Tan, H.; Chen, W.; Liu, D.; Li, Y.; Wang, E. *Dalton Trans.* **2010**, *39*, 1245. (b) Tan, H. Q.; Chen, W. L.; Liu, D.; Wang, E. B. *J. Cluster Sci.* **2010**, *21*, 147. (c) Tan, H. Q.; Chen, W. L.; Liu, D.; Li, Y. G.; Wang, E. B. *Cryst. Eng. Commun.* **2010**, *12*, 4017. (d) Compain, J. D.; Mialane, P.; Marrot, J.; Sécheresse, F.; Zhu, W.; Oldfield, E.; Dolbecq, A. *Chem.—Eur. J.* **2010**, *16*, 13741. (e) Compain, J. D.; Deniard, P.; Dessapt, R.; Dolbecq, A.; Oms, O.; Sécheresse, F.; Marrot, J.; Mialane, P. *Chem. Commun.* **2010**, *46*, 7733. (f) Tan, H.; Chen, W.; Liu, D.; Feng, X.; Li, Y.; Yan, A.; Wang, E. *Dalton Trans.* **2011**, *40*, 8414.

(8) Altermatt, D.; Brown, I. D. *Acta Crystallogr.* **1985**, *B41*, 244.

(9) Henry, M. *J. Cluster Sci.* **2002**, *13*, 437.

(10) Velde, G. T.; Bickelhaupt, F. M.; Baerends, E. J.; Guerra, C. F.; Van Gisbergen, S. J. A.; Snijders, J. G.; Ziegler, T. *J. Comput. Chem.* **2001**, *22*, 931. Theoretical Chemistry, Vrije Universiteit: Amsterdam, The Netherlands, http://www.scm.com.SCM.

(11) Vanlenthe, E.; Baerends, E. J.; Snijders, J. G. *J. Chem. Phys.* **1993**, *99*, 4597.

(12) (a) Klamt, A. *J. Phys. Chem.* **1995**, *99*, 2224. (b) Klamt, A.; Jonas, V. *J. Chem. Phys.* **1996**, *105*, 9972. (c) Pye, C. C.; Ziegler, T. *Theor. Chem. Acc.* **1999**, *101*, 396.

(13) (a) Becke, A. D. *Phys. Rev. A* **1988**, *38*, 3098. (b) Perdew, J. P. *Phys. Rev. B* **1986**, *33*, 8822. (c) Grimme, S.; Antony, J.; Ehrlich, S.; Krieg, H. *J. Chem. Phys.* **2010**, *132*, 154104. (d) Schipper, P. R. T.; Gritsenko, O. V.; van Gisbergen, S. J. A.; Baerends, E. J. *J. Chem. Phys.* **2000**, *112*, 1344.

(14) (a) Vankova, N.; Heine, T.; Kortz, U. *Eur. J. Inorg. Chem.* **2009**, *34*, 5102. (b) Izarova, N. V.; Vankova, N.; Banerjee, A.; Jameson, G. B.; Heine, T.; Schinle, F.; Hampe, O.; Kortz, U. *Angew. Chem., Int. Ed.* **2010**, *49*, 7807.

(15) (a) Lopez, X.; Fernandes, J. A.; Romo, S.; Paul, J. F.; Kazansky, L. P.; Poblet, J. M. *J. Comput. Chem.* **2004**, *25*, 1542. (b) Bagno, A.; Bonchio, M.; Autschbach, J. *Chem.—Eur. J.* **2006**, *12*, 8460.

(16) Sheldrick, G. M. *Acta Crystallogr.* **2007**, *A64*, 112.

(17) Sheldrick, G. M. *SADABS*; University of Göttingen: Göttingen, Germany, 1996.

(18) Rao, D. V. N. S.; Dandala, R.; Narayanan, G. K. A. S. S.; Lenin, R.; Sivakumaran, M.; Naidu, A. *Synth. Commun.* **2007**, *37*, 4359.

■ NOTE ADDED AFTER ASAP PUBLICATION

This paper was published on the Web on October 17, 2011. Due to a production error, numerous text errors were present. The corrected version was reposted on October 21, 2011.